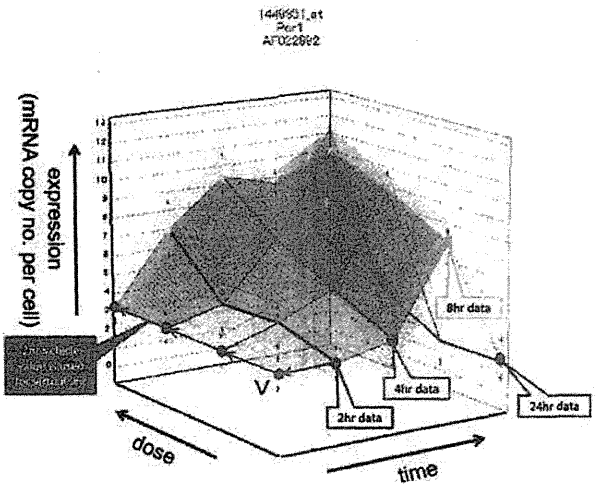

Fig. 1. Three dimensional surface expressions of Percellome Project data: The project data consist of four dose levels and four time points, generating 4 x 4 matrix. The mean value and standard deviation were calculated from the triplicate data. In order to better visualize the changes at 2 hr, the vehicle value was used for zero hour data to draw a 5 x 4 surface graph with X-axis for dose, Y for time, and Z for expression. Here, Affymetrix ID 1449851_at (Per1, period homolog 1) is shown. The 5 x 4 mesh made by the mean values was painted in translucent green (mean surface). The mean surface is rainbow-colored from blue, green, red to yellow according to its peak absolute values (cf. Fig. 3, Supplementary Fig. 1). Above and below the mean surface, +1sd and -1sd surfaces were overlaid using transparent blue. The dose-response curve at 2 hr, 4 hr, 8 hr and 24 hr are highlighted in blue, green, yellow and red. In a direction perpendicular to the dose-response curves, time course of each dose groups and vehicle group is indicated (not highlighted). The graph reads that the highest dose peaked at 4 hr at around 9 copies per cell; the middle dose peaked at 8 hr above 10 copies per cell. The vehicle group (V) showed the circadian change and peaked at 8 hr. The small red crosses are data of each animal sample (n = 3). Yellow asterisks indicate that the marked mean values were significantly different from concurrent vehicle value by $p < 0.05$ (Student's t-test).

Comprehensive selection of treatment-responding mRNAs

The in house developed software, RSort (Roughness Sort by K.A.) was used for automatic selection of treatment-responding mRNAs. This program sorts the PSs based on the roughness of the 3D surface. In other words, calculate the numbers of peaks (upward and downward) in a surface and sort by the number of peaks (maximum of eight peaks in 4 x 4 grid of the surface). Next, it filters the PSs by the number of peaks (normally three or less peaks) and additional parameters such as maximum expression level (normally more than one copy per cell for liver samples), p values between vehicle and top dose groups ($P < 0.05$ or $p < 0.01$). Here, a surface was selected when it had three peaks or less, the first peak in high doses (at any time) or the first peak in middle doses if its value is not significantly different from the neighboring high dose at $p < 0.01$ by Student's t-test, and the value of the peak is significantly different from that of vehicle control at $p < 0.05$ by Student's t-test. These automatically selected PSs were then visually checked for their 3D-surface shapes (to eliminate noisy data), and subdivided into those showed initial changes at 2, 4, 8, and 24 hr. A cross-referencing program named PE (Percellome Explorer, by K.A.) was used to select a list of chemicals that share PSs common to the visually confirmed list of PCP. The PE contains the gene lists automatically selected by the RSort of all data in our Percellome Project (168 datasets for liver samples, 286 for all samples), and automatically cross-refers and sorts out the chemicals sharing the same PSs (Fig. 2). The automatically selected gene lists (product sets) were visually checked to remove noise surfaces.

In Situ Hybridization

For *in situ* hybridization of Irf7 and Stat1 mRNAs, QuantiGeneViewRNA ISH Tissue Assay kit (Affymetrix, Inc., Santa Clara, CA, USA) was used. The probes were designed and synthesized by Affymetrix; regions covered were 2-1461 bases for Irf7 and 707-1710 bases for Stat1. 10% buffered formalin fixed liver tissues were dehydrated and embedded in paraffin. Tissue sections were mounted on "FRONTIER coated glass slides" (Matsunami Glass Ind., Ltd. Osaka, Japan). The slides were completely dried and stored until use. The slides were re-fixed in 10% formaldehyde for 1 hr at room temperature and washed with PBS and deparaffinized with xylene, pretreated in 1x Pretreatment Solution at 98°C for 30 min and digested with Protease QF at 40°C for 20 min. The probes were hybridized at 40°C for 2 hr and the signals were detected with Fast Red.

RESULTS

The numbers of PSs that started to change in response to PCP treatment at 2, 4, 8 and 24 hr were 98, 55, 127 and 1192 respectively (Supplementary Table 2, Supplementary Fig. 1). Chemicals or treatment in the Percellome database (Supplementary Table 1), that shared the PS list with PCP are shown in Table 1. The chemicals that shared the most with the 2 hr PS list of PCP

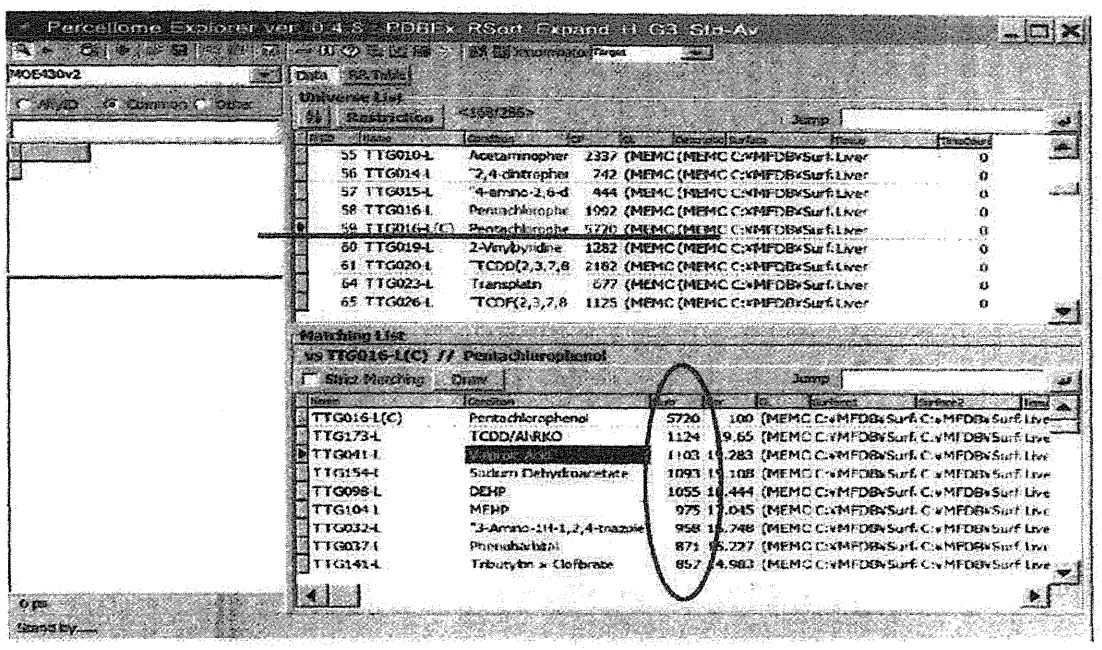

Fig. 2. PercellomeExplorer (PE) Software: The PE contains the gene lists automatically selected by the RSort software program of all data in our Percellome Project (168 datasets for liver samples, 286 for all samples, as of May 2013), and automatically picks up the chemicals sharing same PSs. TTG016-L(C), the study code for PCP was selected from the upper window and the chemicals sharing the PSs were listed in the lower window. These lists await visual confirmation.

was sodium dihydroacetate (TTG154-L); 51 PSs, followed by acephate (TTG109-L); 24 PSs, down to 5-fluorouracil (TTG160-L); 4 PSs. The sum set (or union of sets in set theory) of the 2 hr PS lists that are listed in the 2 hr column of the Table 1 contained 75 PSs (up-regulated (Up) 59, down-regulated (D) 16). Likewise, the sum set of the 4 hr PS lists contained 31 PSs (Up 22, D 9), 8 hr 46 PSs (Up 23, D 23) and 24 hr 636 PSs (all Up). The PS list unique to PCP (Unique list) at each time point contained 23, 24, 81, and 556 PSs at each time points (cf. Supplementary Table 2).

Profiles of genes changed at 2, 4 and 8 hr

The PS list common to other chemicals (Common list) contained the gluconeogenesis pathway of PGC-1A (Ppargc1a)/Foxo1/HNF4 (Puigserver *et al.*, 2003) that were induced at 2 hr (Fig. 3). This finding is in concordance with the report in experimental animals that PCP acutely induces hyperglycemia (Deichman *et al.*, 1942; Clayton and Clayton, 1981). Ppargc1a was reported to increase the expression of Lpin1 (Finck *et al.*, 2006), which was also the case here. A small set of genes encoding metabolic enzymes was induced during the first 8 hr, including Cyp2a4, Cyp4f16, Cyp7a1, Cyp17a1, Cyp39a1, Fmo2, and Fmo5 (Fig. 3).

Ingenuity pathway analysis (Ingenuity Systems, Inc. Redwood City, CA, USA) indicated that these genes are likely to be induced by Nr1i3 (CAR), Nr1i2 (PXR/SXR) or Nr5a1 (data not shown). Although our RSort program did not identify these nuclear receptors, manual search showed that PXR/SXR was induced by PCP (Fig. 3). These changes were not unique to PCP and shared by some of the chemicals in the Common list (cf. Supplementary Table 2).

Down regulation of Fos and JunB at 2, 4, and 8 hr (Fig. 3) was uniquely found in the PCP gene list. Bioinformatic analysis did not identify any associated pathways.

Profiles of genes started to change at 24 hr

The list of PSs induced at 24 hr contained two large networks. About half of the PSs showing altered expression by PCP were assigned to the interferon signaling pathway (Fig. 4, Supplementary Fig. 1). The interferon signaling genes (ISG) were highly up-regulated from Stat1, Stat2, Tyk, to Irf7, Myd88, Oas, Ifit, Cxcl10 and other downstream targets. Toll like receptors (TLRs) and

Table 1. The total numbers of probesets induced by PCP at each time points and those shared with other chemicals.

2 hr			4 hr			8 hr			24 hr		
Percellome No.	Treatment	PS	Percellome No.	Treatment	PS	Percellome No.	Treatment	PS	Percellome No.	Treatment	PS
TTG016-L(C)	Pentachlorophenol	98	TTG016-L(C)	Pentachlorophenol	55	TTG016-L(C)	Pentachlorophenol	127	TTG016-L(C)	Pentachlorophenol	1192
TTG154-L	Sodium Dehydroacetate	51	TTG104-L	MEHP	21	TTG098-L	DEHP	15	TTG098-L	DEHP	258
TTG109-L	Acephate	24	TTG098-L	DEHP	16	TTG041-L	Valproic Acid	14	TTG032-L	3-Amino-1H-1,2,4-triazole	212
TTG059-L	Caffeine	19	TTG037-L	Phenobarbital	14	TTG104-L	MEHP	14	TTG104-L	MEHP	177
TTG062-L(C)	Dexamethasone	18	TTG032-L	3-Amino-1H-1,2,4-triazole	12	TTG109-L	Acephate	13	TTG037-L	Phenobarbital	160
TTG041-L	Valproic Acid	18	TTG144-L	[illegible]	12	TTG160-L	5-fluorouracil	10	TTG041-L	Valproic Acid	109
TTG098-L	DEHP	17	TTG150-L	Valproic acid sodium salt x Thalidomide	8	TTG154-L	Sodium Dehydroacetate	9	TTG157-L	[illegible]	103
TTG019-L	2-Vinylpyridine	15	TTG141-L	Tributyltin x Clofibrate	8	TTG141-L	Tributyltin x Clofibrate	8	TTG031-L	2,4-Diamino-6,7-dimethylpteridine	94
TTG104-L	MEHP	12	TTG074-L	[illegible]	8	TTG031-L	2,4-Diamino-6,7-dimethylpteridine	8	TTG154-L	Sodium Dehydroacetate	77
TTG165-L	Chlorpyrifos	12	TTG151-L	Valproic acid sodium salt x Valproic acid sodium salt	7	TTG032-L	3-Amino-1H-1,2,4-triazole	8	TTG162-L	[illegible]	71
TTG034-L	[illegible]	12	TTG031-L	2-Chloro-2'-deoxyadenosine	7	TTG146-L	Forskolin	6	TTG044-L	[illegible]	69
TTG166-L	[illegible]	10	TTG044-L	[illegible]	6	TTG062-L(C)	Dexamethasone	6	TTG074-L	[illegible]	47
TTG031-L	2,4-Diamino-6,7-dimethylpteridine	10	TTG162-L	[illegible]	5	TTG054-L	Diethylnitrosamine (C57BL/6)	5	TTG109-L	Acephate	17
TTG141-L	Tributyltin x Clofibrate	9				TTG132-L	Curcumin	3	TTG160-L	5-fluorouracil	13
TTG032-L	3-Amino-1H-1,2,4-triazole	9				TTG136-L	[illegible]	2			
TTG027-L	1,2,3-Triazole	9									
TTG160-L	5-fluorouracil	4									
	Sum Set (common)	75		Sum Set (common)	31		Sum Set (common)	46		Sum Set (common)	636
	Sum Set (Up)	59		Sum Set (Up)	22		Sum Set (Up)	23		Sum Set (Up)	636
	Sum Set (Dn)	16		Sum Set (Dn)	9		Sum Set (Dn)	23		Sum Set (Dn)	0
	PCP NOT Sum (unique to PCP)	23		PCP NOT Sum (unique to PCP)	24		PCP NOT Sum (unique to PCP)	81		PCP NOT Sum (unique to PCP)	556

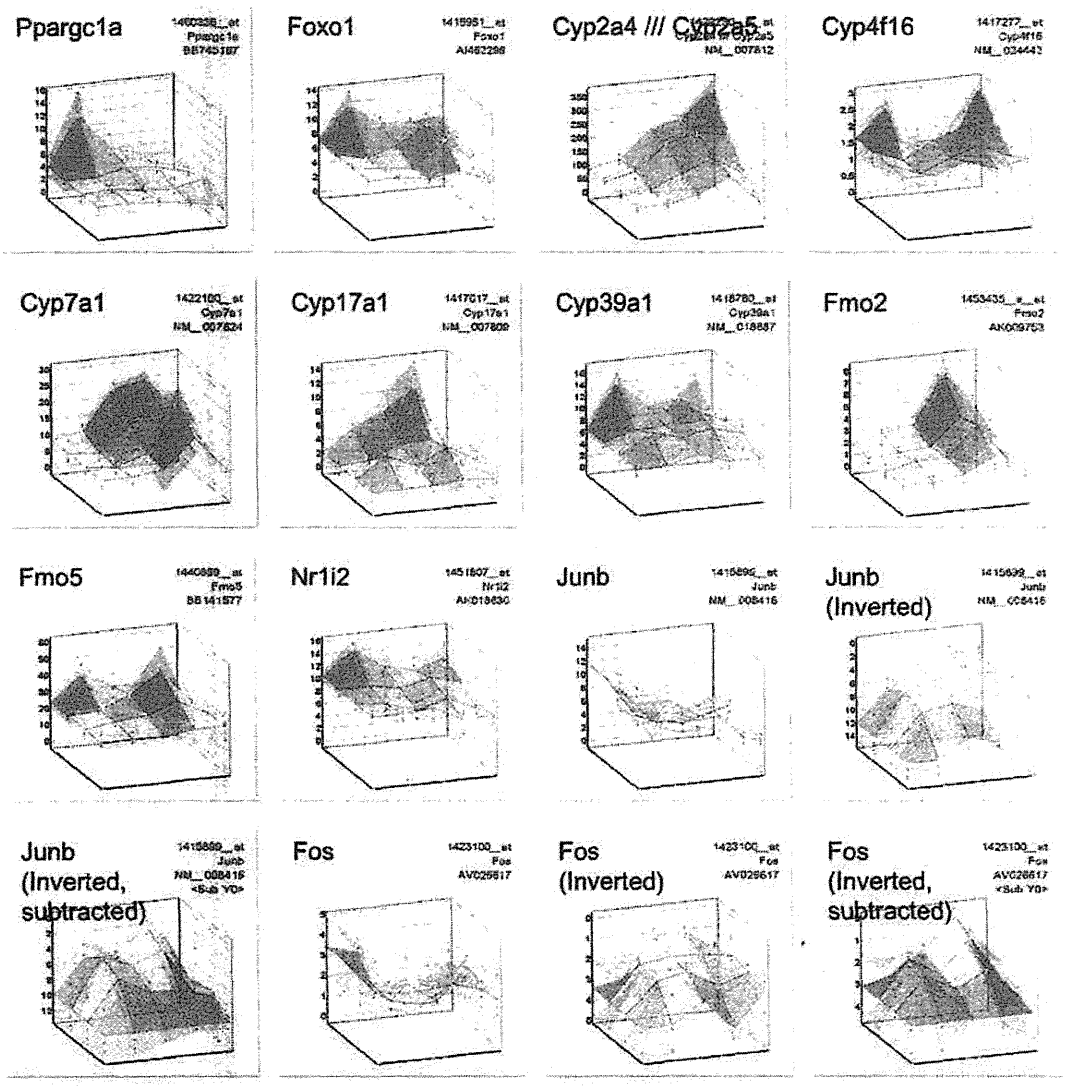

Fig. 3. Representative surface data of PSs induced at 2, 4 and 8 hr after PCP single gavage: Ppargc1a and Foxo1 are the members of gluconeogenesis pathway. A small set of genes of metabolic enzymes, such as Cyp2a4, Cyp4f16, Cyp7a1, Cyp17a1, Cyp39a1, Fmo2, and Fmo5 are induced during the first 8 hr. Nr1i2 or PXR/SXR is also induced. Down regulation of JunB and Fos at 2, 4, and 8 hr are noted. The graphs marked with (Inverted) are plotted with inverted z-axis, zero on top for better indication of suppression. The graphs with (Inverted, subtracted) are plotted, in addition to inverted z-axis, with the 2, 4, 8 and 24 hr values compensated by concurrent vehicle values so that the vehicle line is straight and cancels out the circadian changes.

other pattern recognition receptors (PRR), interferon regulatory factors (Irf) and interferon (Ifn) itself were included. These ISGs were uniquely induced by PCP. It is notable that inflammatory cytokines such as Tnf-α, IL-12 and CD40 were not effectively induced by PCP. The Ingenuity Pathways also plotted many genes in the interferon signaling with a very high probability score (Fig. 6).

In situ hybridization confirmed that hepatocytes were producing the Irf7 and Stat1 in a dose dependent manner (Fig. 7, only vehicle and top dose were shown).

The other half was assigned, by Ingenuity Pathway analysis, to Nrf2-mediated Oxidative Stress Responses

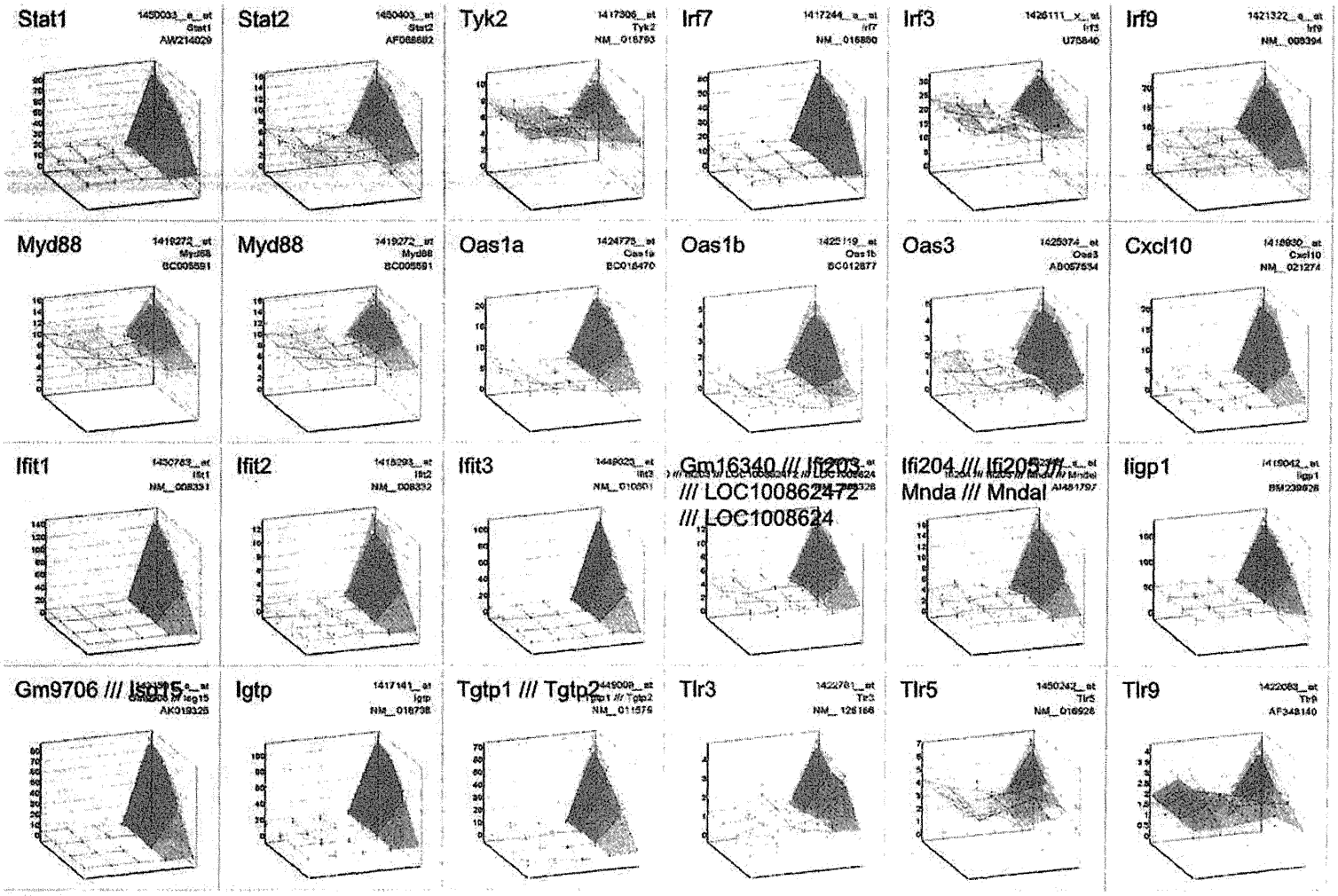

Fig. 4. Surface data of ISGs: Among about 1,200 PSs induced at 24 hr, half of them were uniquely induced by PCP and were assigned to ISG pathway from Stat1, Stat2, Tyk, to Irf7, Myd88, Oas, Ifit, Cxcl10 and other downstream targets. Some Tlrs were also uniquely up-regulated (cf. Supplementary Table 2).

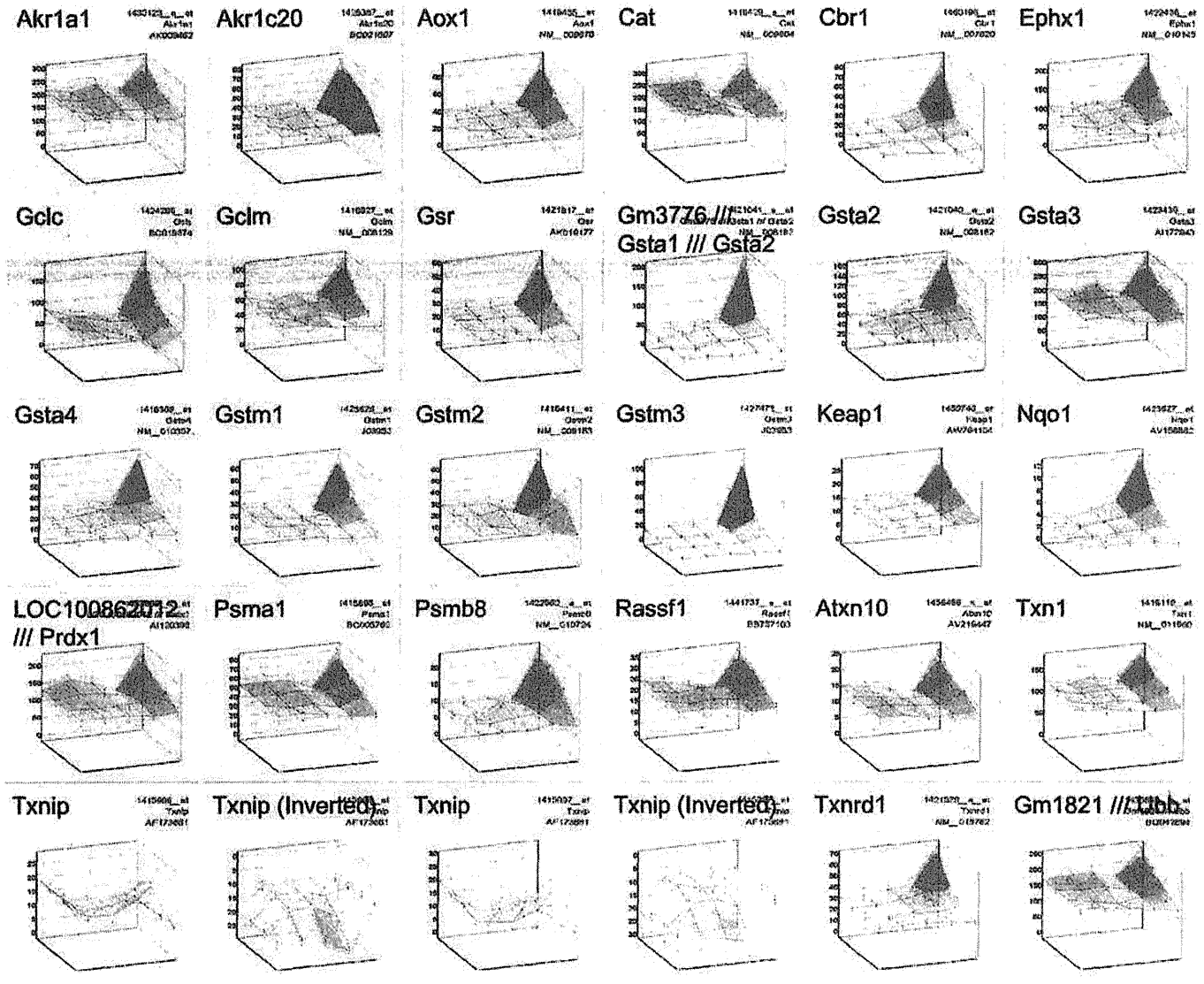

Fig. 5. Surface data of Nrf2-mediated oxidative stress response genes: Among about 1,200 PSs induced at 24 hr, another half of them were Nrf2-mediated oxidative stress response genes commonly induced by PCP and other 10 or so chemicals (cf. Supplementary Table 2). Nrf2 itself did not alter but Keap1 was clearly induced.

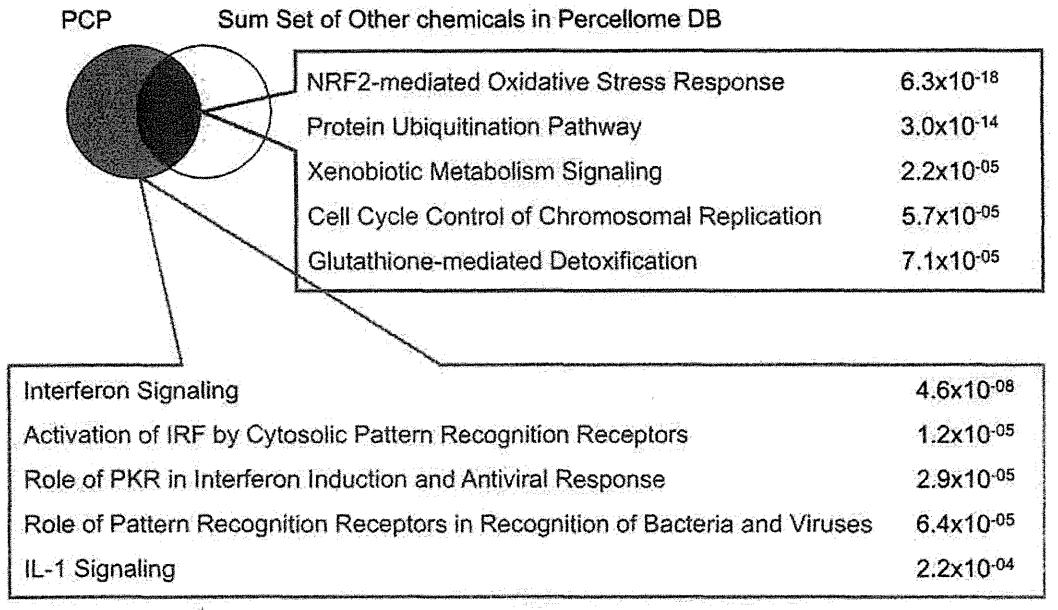

Fig. 6. Venn diagram of the PSs of PCP and sum set of other chemicals in Percellome Database. The PS list unique to PCP was assigned to Interferon signaling and related networks. The PSs induced by PCP and were shared by other chemicals in Percellome database were enriched in Nrf2-mediated oxidative stress response and Protein ubiquitination pathways. The names of the responses and their probability scores are generated by the Ingenuity Pathway analysis.

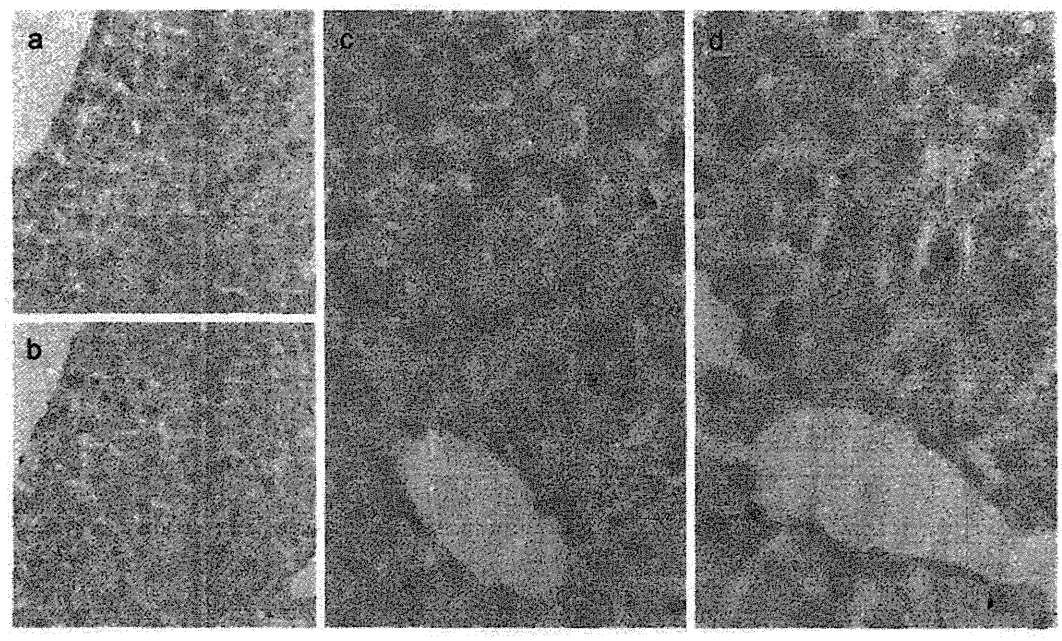

Fig. 7. *In situ* hybridization of Irf7 and Stat1. a) Vehicle control liver stained for Irf7. In a very low back ground, a small nest of hepatocytes was positively stained for Irf7. b) Vehicle control liver stained for Stat1. In a very low back ground, a small nest of hepatocytes was positively stained for Irf7. It is likely that the same hepatocyte is producing both mRNAs. c, d) High dose group stained for Irf7 and Stat1. Hepatocytes were shown to produce both mRNAs in a ubiquitous manner.

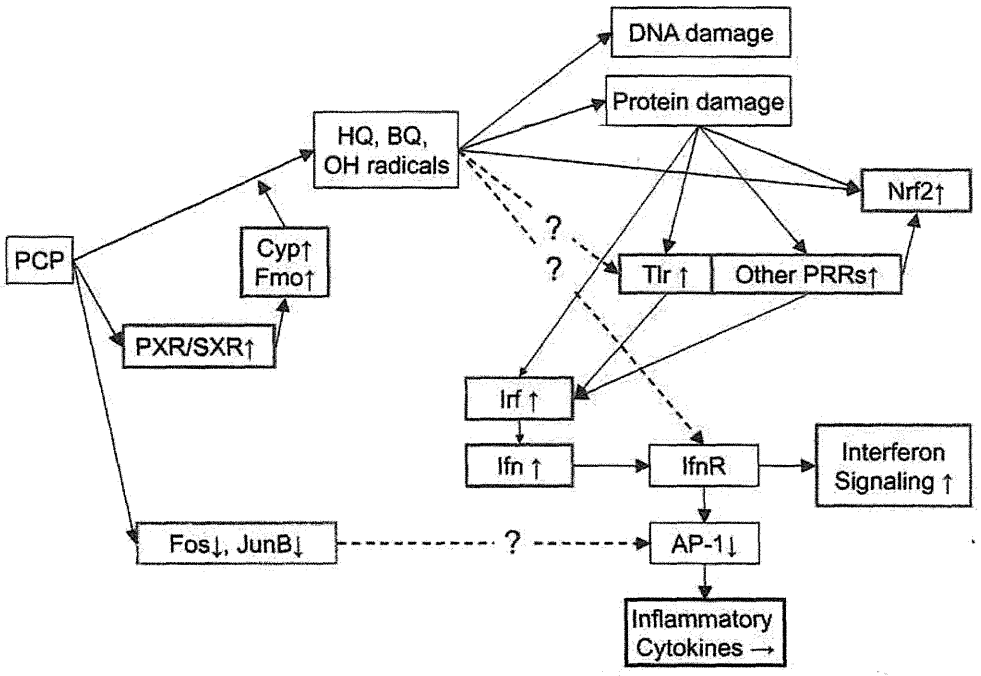

Fig. 8. Tentative summary scheme of the PCP induced networks in mouse liver. PCP or its metabolites may stimulate PXR/SXR or CAR, thereby inducing Cyp2, 4, 7, Fmo2, 5 within 8 hr to facilitate PCP metabolism, generating HQ (TCoHQ,TCpHQ), BQ (TCpBQ) and hydroxyl radical. The metabolites/radicals induce DNA damage and Protein damage. These reaction triggers Nrf2 networks and PRR system, initiating Irf mediated synthesis of Interferon alpha, which triggers the interferon signaling networks by autocrine or paracrine mechanisms. On the other hand, there remains a possibility that the metabolites may act as direct ligands to Tlr or IfnR and trigger downstream events as indicated in dotted lines with "?". Before activating interferon signaling networks, PCP suppressed Fos and JunB, which might have suppressed the inflammatory cytokine induction as shown in dotted line with "?".

accompanying distinct induction of Keap1, and other metabolic pathways (Figs. 5 and 6, Supplementary Table 1). Those networks were in the Common list mentioned above. Other networks were not effectively identified by the Ingenuity pathway analysis.

DISCUSSION

Among the chemicals tested in the Percellome project, PCP was slow to induce changes in gene expression; only around one hundred PSs were induced before 8 hr and 1,200 PSs at 24 hr. It would be plausible to hypothesize that PCP was metabolized during the first 8 hr and that the metabolite(s) then induced the 24 hr burst of ISGs and Nrf2-mediated genes. The time course of PCP action is in accord with the reported biological half-life of PCP; 6 to 27 hr in rodents (Larsen *et al.*, 1972; Braun *et al.*, 1977). A few metabolizing enzymes located downstream of PXR/SXR were induced during the first 8 hr (Fig. 3). The presence of DEHP in the top part of the common chemical list in Table 1 is also consistent with this hypothesis.

It would be of interest to ascertain whether PCP or its metabolite(s) could be PXR/SXR ligands. Metabolites known are tetrachloro-p(o)-hydroquinone (TCpHQ and TCoHQ) and tetrachloro-p-benzoquinone (chloranil, TCpBQ). Further, TCpHQ is reported to be metabolized, generating hydroxyl radicals with a help of H_2O_2 without Fenton reaction, to trichloro-hydroperoxyl-1,4-benzoquinone (TrCBQ-OOH) and trichloro-hydroxy-1,4-benzoquinone (TrCBQ-OH) (Zhu and Shan, 2009). We have no Percellome data of those metabolites and, to date, there are no reports on the interaction of PCP or its metabolites with the PXR/SXR. There are reports that PCP affects the function of estrogen receptor (Jung *et al.*, 2004) and thyroid hormone receptor (Kawaguchi *et al.*, 2008). Further study will be needed to identify the triggering event for the earliest responses to PCP.

Bone 60 (2014) 68–77

Contents lists available at ScienceDirect

Bone

journal homepage: www.elsevier.com/locate/bone

Original Full Length Article

Estrogen receptor α in osteocytes regulates trabecular bone formation in female mice

Shino Kondoh [a], Kazuki Inoue [a,b,c], Katsuhide Igarashi [d], Hiroe Sugizaki [e], Yuko Shirode-Fukuda [a], Erina Inoue [a], Taiyong Yu [a,b], Jun K. Takeuchi [e,f], Jun Kanno [d], Lynda F. Bonewald [g], Yuuki Imai [a,b,*]

[a] Laboratory of Epigenetic Skeletal Diseases, Institute of Molecular and Cellular Biosciences, The University of Tokyo, Tokyo, Japan
[b] Division of Integrative Pathophysiology, Proteo-Science Center, Graduate School of Medicine, Ehime University, Ehime, Japan
[c] Department of Biological Resources, Integrated Center for Science, Ehime University, Ehime, Japan
[d] Division of Cellular & Molecular Toxicology, Biological Safety Research Center, National Institute of Health Sciences, Tokyo, Japan
[e] Division of Cardiovascular Regeneration, Institute of Molecular and Cellular Biosciences, The University of Tokyo, Tokyo, Japan
[f] JST PRESTO, Japan
[g] Department of Oral Biology, School of Dentistry, University of Missouri at Kansas City, Kansas City, MO, USA

ARTICLE INFO

Article history:
Received 8 July 2013
Revised 26 November 2013
Accepted 4 December 2013
Available online 10 December 2013

Edited by: Shu Takeda

Keywords:
Estrogen
Estrogen receptor α
Osteocyte
Bone formation
Wnt signaling

ABSTRACT

Estrogens are well known steroid hormones necessary to maintain bone health. In addition, mechanical loading, in which estrogen signaling may intersect with the Wnt/β-catenin pathway, is essential for bone maintenance. As osteocytes are known as the major mechanosensory cells embedded in mineralized bone matrix, osteocyte ERα deletion mice ($ER\alpha^{\Delta Ocy/\Delta Ocy}$) were generated by mating ERα floxed mice with Dmp1-Cre mice to determine the role of ERα in osteocytes. Trabecular bone mineral density of female, but not male $ER\alpha^{\Delta Ocy/\Delta Ocy}$ mice was significantly decreased. Bone formation parameters in $ER\alpha^{\Delta Ocy/\Delta Ocy}$ were significantly decreased while osteoclast parameters were unchanged. This suggests that ERα in osteocytes exerts osteoprotective function by positively controlling bone formation. To identify potential targets of ERα, gene array analysis of Dmp1-GFP osteocytes sorted by FACS from $ER\alpha^{\Delta Ocy/\Delta Ocy}$ and control mice was performed. Gene expression microarray followed by gene ontology analyses revealed that osteocytes from $ER\alpha^{\Delta Ocy/\Delta Ocy}$ highly expressed genes categorized in 'Secreted' when compared to control osteocytes. Among them, expression of Mdk and Sostdc1, both of which are Wnt inhibitors, was significantly increased without alteration of expression of the mature osteocyte markers such as Sost and β-catenin. Moreover, hindlimb suspension experiments showed that trabecular bone loss due to unloading was greater in $ER\alpha^{\Delta Ocy/\Delta Ocy}$ mice without cortical bone loss. These data suggest that ERα in osteocytes has osteoprotective functions in trabecular bone formation through regulating expression of Wnt antagonists, but conversely plays a negative role in cortical bone loss due to unloading.

Published by Elsevier Inc.

Introduction

Estrogens clearly maintain physiological homeostasis through the development of reproductive organs and the mammary gland, potentiation of muscles, and through osteoprotection. The osteoprotective actions of estrogens are clearly demonstrated by post-menopausal osteoporosis [1]. The effects of sex steroid hormones on bone tissue can be considered as the combination or sum of the direct effects on bone cells and the indirect effects on other tissues [2]. The indirect effects of estrogen on bone through other tissues have been well described, such as modulation of cytokine production by immune cells and the increased induction of pituitary gland hormones [3,4]. However, the direct effect of estrogens on bone tissue is not fully understood.

Estrogens exert their effects by binding to their own nuclear receptors, such as Estrogen Receptor (ER) α and β, which also function as transcription factors. The conventional ERα null mouse model could not be used to address the direct functions of the receptor in bone due to hormonal imbalance and endocrine disturbances [5–7]. Therefore, the generation and analyses of bone cell type specific deletion is required to clarify the functions of ERα in bone.

Osteoclastic ERα null mice were generated showing that osteoclastic ERα shortens the life span of osteoclasts by promoting apoptosis [8,9]. Ovariectomy can induce osteocyte apoptosis [10] and conventional ERα null mice do not increase bone mass in response to anabolic mechanical loading [11]. Moreover, various groups reported murine skeletal phenotype due to ERα deletion in cells of the osteoblast lineage, suggesting ERα in osteoblastic lineage cells could play important roles in the maintenance of bone metabolism [12–15]. Recently, Windahl

* Corresponding author at: Division of Integrative Pathophysiology, Proteo-Science Center, Graduate School of Medicine, Ehime University, Shitsukawa, Toon, Ehime 791-0295, Japan. Tel.: +81 89 960 5925; fax: +81 89 960 5953.
E-mail address: y-imai@m.ehime-u.ac.jp (Y. Imai).

8756-3282/$ – see front matter. Published by Elsevier Inc.
http://dx.doi.org/10.1016/j.bone.2013.12.005

et al. [13] reported that ERα in osteocytes regulates trabecular bone formation and thus trabecular bone volume in male mice. These results are in contrast to our own findings showing that the precise molecular functions and target genes of ERα in osteocytes still remain elusive.

Osteocytes are embedded in the extracellular matrix of bone and represents more than 90% of the cells existing in bone. Osteocytes possess dendrites that extend throughout the bone and are used to communicate with each other and also with osteoblasts and osteoclasts on the surface of the bone. The function of osteocytes as mechanosensory cells is inferred from their shape and location [16]. In fact, mechanical loading and unloading change osteocyte gene expression *in vivo*, indicating that osteocyte function is affected by loading conditions [17–20]. In addition, they are known to be involved in mineral metabolism through expression of proteins such as FGF23, Phex, Mepe, and Dmp1 [21–24] (for review, see [25]). Recently, it has been postulated that osteocytes can orchestrate skeletal homeostasis through mineral metabolism as well as the regulation of osteoblastic bone formation and osteoclastic bone resorption by secretory proteins such as sclerostin and FGF23. Osteocytes are also reported to regulate osteoblastic bone formation through IGF-1, TGFβ, NO, PGE_2 and sclerostin and to regulate osteoclastic bone resorption through TGFβ, NO, and PGE_2, and RANKL/OPG [26].

Bone mass can be maintained by mechanical loading while unloading or immobilization decreases bone mass. *In vivo* unloading rodent models such as tail suspension can induce bone loss in hind limbs [27] and mechanical loading can increase bone mass in forelimbs [28]. The regulation of bone mass by mechanical loading is mediated, at least in part, through β-catenin signaling [29–31], and estrogen/ER signaling might also be involved in this mechanism [32].

In this study, we examined the functions of ERα in osteocytes by generating mice lacking ERα in osteocytes and analyzing osteocyte gene expression profiles and subjecting them to hindlimb unloading.

Materials and methods

Animals

The ERα floxed mutant ($ER\alpha^{L2/L2}$) mice kindly provided by Dr. Chambon and null alleles with a C57BL/6 J background have been previously described [5]. $ER\alpha^{L2/L2}$ mice were crossed with $Dmp1^{Cre}$ mice [33] to generate $Dmp1^{Cre}$; $ER\alpha^{L2/+}$ mice, and $Dmp1^{Cre}$; $ER\alpha^{L2/L2}$ ($ER\alpha^{\Delta Ocy/\Delta Ocy}$) and $ER\alpha^{L2/L2}$ ($ER\alpha^{flox/flox}$) were obtained by crossing $Dmp1^{Cre}$; $ER\alpha^{L2/+}$ and $ER\alpha^{L2/L2}$. *Dmp1-GFP* mice were kindly provided by Dr. Ivo Kalajzic [34]. All mice were housed in a specific-pathogen-free facility under climate-controlled conditions with a 12-hour light/dark cycle and were provided with water and standard diet (CE-2, CLEA, Japan) *ad libitum*. All animals were maintained and examined according to the protocol approved by the Animal Care and Use Committee of the University of Tokyo.

Genome DNA extraction and cell culture

Various tissues (0.5 g) from $ER\alpha^{\Delta Ocy/\Delta Ocy}$ were harvested, washed with PBS and lysed in 2 ml of lysis buffer with proteinase K (150 μg/ml) overnight. Also, DNA of osteocytes was isolated from the calvariae of $ER\alpha^{\Delta Ocy/\Delta Ocy}$ in which cells on the surface of the bone such as osteoclasts and osteoblasts were removed by sequential enzymatic treatment. Primary osteoblasts obtained from the neonatal calvariae were cultured in αMEM (Life Technologies) containing 10% FBS (Cell Culture Bioscience), 50 μg/ml ascorbic acid (Sigma-Aldrich) and 10 nM β-glycerophosphate (Sigma-Aldrich) for 21 days. Cells were cultured with phenol red free media 24 h before cells were treated with 17β-estradiol. Primary osteoclasts were differentiated from the bone marrow obtained from 6-week-old $ER\alpha^{\Delta Ocy/\Delta Ocy}$ mice using 10 ng/ml of M-CSF (R&D Systems) and 234 ng/ml of GST-RANKL (Oriental Yeast) for 5 days. The genomic DNA was extracted using phenol/chloroform and isopropanol precipitation.

ELISAs

Enzyme-linked Immunoassays, ELISAs, were was performed following the protocols of the Estradiol EIA Kit (Cayman Chemical Company) for estradiol, Testosterone EIA Kit (Cayman Chemical Company) for testosterone, and Rodent Luteinizing Hormone (LH) ELISA TEST (Endocrine Technologies) for LH.

Bone analyses

The BMD of femurs and tibiae obtained from 12-week-old littermates were measured by DXA using a bone mineral analyzer (DCS-600EX: ALOKA). Micro Computed Tomography scanning of the tibiae and femurs was performed using a Scanco Medical μCT35 System (SCANCO Medical) with an isotropic voxel size of 6 μm for trabecular analyses and 12 μm for cortical analyses according to the manufacturer's instructions and the recent guidelines of the American Society for Bone and Mineral Research (ASBMR) [35]. For bone histomorphometry, the mice were double-labeled with intra-peritoneal injections of 16 mg/kg of calcein (Sigma) at 5 and 2 days before sacrifice. Lumbar vertebral bodies were removed from each mouse and fixed with 4% PFA in PBS overnight. Lumbar vertebrae were embedded with MMA after dehydration and the plastic sections were cut by a standard microtome (LEICA) into 7 μm for von Kossa staining and 4 μm for TRAP and Toluidine-blue staining. The region of interest was the secondary spongiosa of L3 and L4. Sections were used for analyses when the bases of the bilateral transverse processes were opened. The region of interest (ROI) in the lumbar vertebral body is the secondary spongiosa, which is separated from the primary spongiosa, cranial and caudal growth plate, according to the same protocol as previously performed [8,36]. Histomorphometric analyses were performed using OsteoMeasure (OsteoMetrics, Inc., GA, USA) according to the ASBMR guideline [37].

Isolation of Dmp1-GFP positive osteocytes by FACS

A highly purified population of osteocytes was isolated from neonatal calvariae by FACS using a modified version of the protocol of Paic F et al. [38]. Cells were isolated from 10-day-old fetal mice calvariae of $ER\alpha^{\Delta Ocy/\Delta Ocy}$ and $ER\alpha^{flox/flox}$ also expressing *Dmp1-GFP*. After removal of the sutures, pooled calvarial tissue was subjected to six sequential, 30-minute digestions in a mixture containing 0.05%/0.2 mM trypsin/EDTA and 1.5 U/ml collagenase-P (Roche) at 37 °C. Cell fractions 4 to 6 were collected, pooled, and re-suspended in Dulbecco's modified Eagle's medium (DMEM, Life Technologies) containing 10% FBS (Hyclone) and centrifuged. Cells were rinsed with PBS and re-suspended in PBS/2% FBS and filtered through a 70-μm filter. Cell sorting was performed using a BD FACS Aria cell sorter. The gate for collecting GFP+ cells was set as GFP+ population to represent 10% to 15% of the total cells in GFP+ mice and 0.8% to 1.0% of total cells in GFP− mice (negative control). GFP+ cells were collected in a tube with 500 μl of PBS/3% FBS.

Gene expression microarray

Gene expression microarray was generated using total RNA extracted from the isolated GFP+ osteocytes of $ER\alpha^{\Delta Ocy/\Delta Ocy}$ and $ER\alpha^{flox/flox}$ as previously described [8] and RNA samples were evaluated using the Affymetrix Mouse Genome 430 2.0 Array following standard Affymetrix protocols (GEO: GSE41997). Gene ontology analyses were performed using DAVID Bioinformatics Resources 6.7 [39].

RNA extraction and RT-qPCR

Total RNA from the pulverized femurs or sorted cells was extracted using TRIZOL (Invitrogen) and RNeasy purification kit (QIAGEN). First-strand cDNA was synthesized from total RNA using PrimeScript RT Master Mix (TaKaRa) and subjected to RT-qPCR using SYBR Premix Ex Taq II